Biomimetic models of [NiFe] hydrogenase for electrocatalytic hydrogen evolution

Gezer, G.

Chapter 5

Synthesis and Characterization of Trinuclear [NiRu] Complexes for Electrocatalytic Proton Reduction

Abstract

Two new trinuclear compounds [{Ni(xbSmS)}$_2$Ru(phen)$_2$](PF$_6$)$_2$ and [{Ni(xbSmSe)}$_2$Ru(phen)$_2$](PF$_6$)$_2$ were synthesized by the reaction of [Ni(xbSmS)] and [Ni(xbSmSe)] with cis-[Ru(phen)$_2$(Cl)$_2$] (H$_2$xbSmS = 1,2-bis(4-mercapto-3,3-dimethyl-2-thiabutyl)benzene; H$_2$xbSmSe = 1,2,-bis(2-thiabutyl-3,3-dimethyl-4-selenol)benzene; phen = phenanthroline). The two [Ni$_2$Ru] complexes were characterized by ESI-MS, NMR, elemental analysis, single crystal X-ray crystallography and electrochemical techniques. X-ray structure determinations showed that the trinuclear complex cations in ***(1)*** *and* ***(2)*** *contain two square-planar nickel centers bound in cis positions to the octahedral ruthenium ion via a bridging thiolate or selenolate donor atom. Electrocatalytic proton reduction occurs for both complexes in acetonitrile with addition of varying amounts of acetic acid at a potential of −2.1 V vs. Fc$^+$/Fc with faradaic yields of around 65%.*

This chapter is submitted for publication: G. Gezer, D. Durán Jiménez, M. A. Siegler, and E. Bouwman.

5.1 Introduction

Molecular hydrogen (H_2) is a perfect candidate as energy carrier to be used as an alternative to fossil fuels. The hydrogen economy relies on the vision of replacing fossil fuels by dihydrogen as a low-carbon energy source.[1] A way of producing dihydrogen gas is via the (electrocatalytic) hydrogen evolution reaction (HER), in which protons are combined with electrons to yield molecular hydrogen as shown in equation 1.[2]

$$2H^+ + 2e^- \rightleftarrows H_2 \qquad [1]$$

In 1930 Stephenson and Stickland reported an enzyme found in certain microorganisms capable of molecular hydrogen activation for which they proposed the name hydrogenase.[3] It was discovered that in microorganisms containing this hydrogenase dihydrogen can be produced or used as a source of electrons in a global H_2 cycle. The hydrogenase family is divided in three classes based on the identity of the metal ions in the active site, the [NiFe], [FeFe] and [Fe] hydrogenases, which catalyze proton reduction or dihydrogen oxidation at very high rates.[4] Many structural and functional models for the active site in [FeFe] hydrogenase have been reported, but especially functional models of the [NiFe] hydrogenases are less mature.[5] In order to produce efficient functional models of the active site of [NiFe] hydrogenases organometallic [NiFe] and even [NiRu] coordination compounds have been prepared.[4] The choice for ruthenium to replace iron in mimicking the active site is based on the fact that ruthenium complexes are active as (homogeneous) catalysts in hydrogenation and hydrogen transfer reactions and generally form more stable coordination compounds. Most significant is the fact that Ru(II) ions are able to accept both hard and soft ligands such as hydride and dihydrogen, which makes it suitable for replacing the Fe center in models of the [NiFe] hydrogenases.[4] In the past decade several heterodinuclear [NiRu] complexes have been reported as structural and functional models of [NiFe] hydrogenases.[6-8,10] A subclass of [NiFe] hydrogenases comprises the [NiFeSe] hydrogenases, in which one of the non-bridging cysteines (Cys) in the active site of the enzyme is replaced by selenocysteine (Sec).[11] Until now only few studies have been directed to mimic the active site of [NiFeSe] hydrogenase using a selenolate ligand coordinated to the nickel center.[12,13]

The aim of this research is the synthesis and characterization of novel electrocatalyst for the reduction of protons to dihydrogen gas. Previously it has been shown that catalysts based on heterodinuclear [NiRu] compounds are very promising electrocatalysts for the HER.[9] The

introduction of large and bulky ligands for steric protection of the ruthenium center in the [NiRu]-based catalysts has been reported to result in increased stability during the catalytic cycle.[9] In this chapter our study is described of two new trinuclear [NiRu] complexes derived from a reaction of the compounds [Ni(xbSmS)][14] and [Ni(xbSmSe)][15] with *cis*-$[Ru(phen)_2(Cl)_2]$ (H_2xbSmS = 1,2-bis(4-mercapto-3,3-dimethyl-2-thiabutyl)benzene; H_2xbSmSe = 1,2,-bis(2-thiabutyl-3,3-dimethyl-4-selenol)benzene; phen = phenanthroline).[16] Both NiS_4 and NiS_2Se_2 complexes are used in order to investigate the effect of changing the sulfur donor atom to selenium, as inspired by the active sites in [NiFe] and [NiFeSe] hydrogenases.

5.2 Results

5.2.1 Synthesis and Characterization

The mononuclear nickel and ruthenium precursor complexes were synthesized following reported procedures.[14,15,16] The novel trinuclear complexes $[\{Ni(xbSmS)\}_2Ru(phen)_2](PF_6)_2$ **(1)** and $[\{Ni(xbSmSe)\}_2Ru(phen)_2](PF_6)_2$ **(2)** were synthesized by refluxing an ethanolic solution of the compound [Ni(xbSmS)] or [Ni(xbSmSe)] with the compound *cis*-$[Ru(phen)_2(Cl)_2]$ and were obtained as dark reddish-brown solids in 43% and 46% yield, respectively (Scheme 5.1). The chloride anions were exchanged with PF_6^- anions using NH_4PF_6. It was our intention to make dinuclear NiRu complexes with two bridging thiolates starting from a 1:1 ratio of the nickel and ruthenium complexes. However, the NMR spectra of the obtained complexes were not in agreement with the expected dinuclear compounds. The crystal structures of the obtained complexes surprisingly showed that trinuclear $[Ni_2Ru]$ complexes were obtained instead. The synthesis of the compounds was then optimized using a 2:1 ratio of the precursor nickel and ruthenium complexes. Both $[Ni_2Ru]$ complexes were characterized by ^{1}H NMR spectroscopy, mass spectrometry, elemental analysis and single crystal X-ray crystallography. Although acetone solutions of both complexes give rise to sharp resonances in the ^{1}H NMR spectra, it is difficult to assign all peaks in the aromatic region. The ESI-MS spectra of the complexes exhibit the parent molecular ion peaks at *m/z* = 633.7 and 727.2 for **(1)** and **(2)** respectively, for the trinuclear dicationic compound $[M-2(PF_6)]^{2+}$.

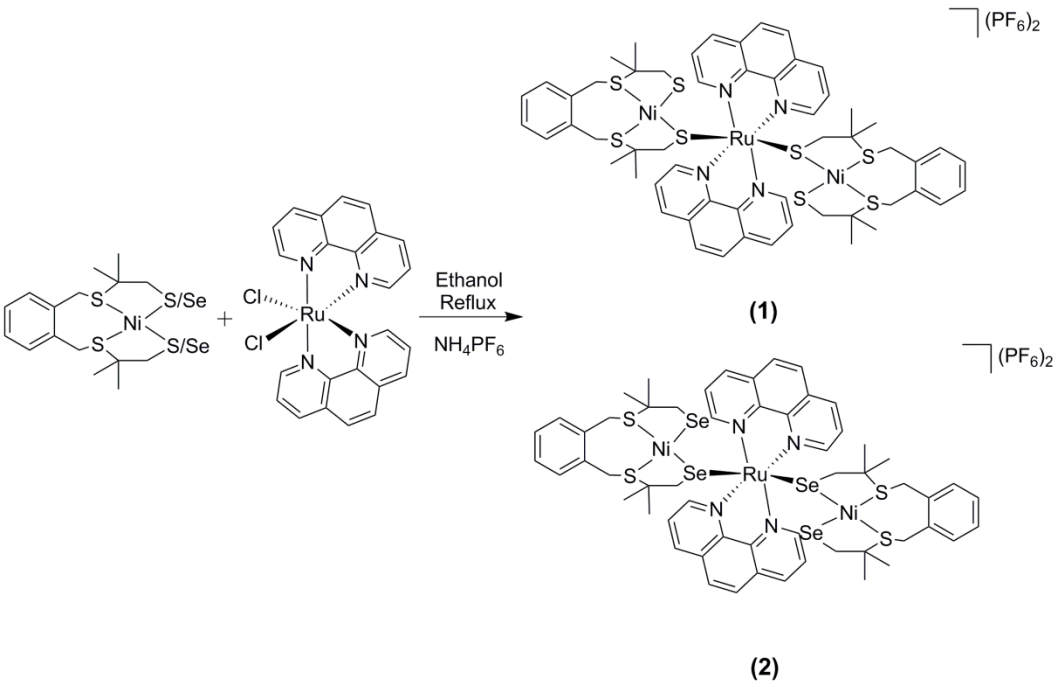

Scheme 5.1: Synthesis scheme of the complexes $[\{Ni(xbSmS)\}_2Ru(phen)_2](PF_6)_2$ **(1)** and $[\{Ni(xbSmSe)\}_2Ru(phen)_2](PF_6)_2$ **(2)**

5.2.2 Description of the Structures

Single crystals of the compounds $[\{Ni(xbSmS)\}_2Ru(phen)_2](PF_6)_2$ **(1)** and $[\{Ni(xbSmSe)\}_2Ru(phen)_2](PF_6)_2$ **(2)** were obtained by vapor diffusion of 2-propanol into acetone solutions of the complexes. Projections of the structures of **(1)** and **(2)** are given in Figure 5.1; selected interatomic distances and angles are provided in Table 5.1. For complex **(1)**, one of the two Ni complexes and one phenanthroline ligand coordinated to Ru are disordered over two orientations. The crystal structure further contains lattice acetone solvent molecules that together with the PF_6^- ions are disordered over two orientations. The crystal lattice of complex **(2)** also contains some amounts of lattice acetone solvent molecules and two PF_6^- ions disordered over two or three orientations. The trinuclear complex cations in **(1)** and **(2)** contain two square-planar nickel centers bound in *cis* positions to the octahedral ruthenium ion via a bridging thiolate or selenolate donor atom with S-Ru-S and Se-Ru-Se angles of 90.80(15)° and 88.969(13)°, respectively. The square-planar coordination environment of the Ni(II) centers comprises two thioether and two thiolate/selenolate donor atoms in mutual cis positions and is slightly distorted with dihedral angles of 12.17° and 16.9°, defined by the planes $S_{thioether}$-Ni-$S_{thioether}$ and $S_{thiolate}$-Ni-$S_{thiolate}$ for complex **(1),** and 9.74° and 12.14° defined by the planes S-Ni-S and Se-Ni-Se for complex **(2)**. The Ru(II)

centers are octahedral, *cis*-coordinated to two thiolate/selenolate ligands. The ruthenium center is also bound to two 1,10-phenanthroline ligands making the metal compound chiral, but due to the centrosymmetric space group both enantiomers are present in the crystal lattice. The Ni-$S_{thiolate}$ and Ni-$S_{thioether}$ distances in complex **(1)** are quite similar, but obviously the Ni-$Se_{selenolate}$ distances in complex **(2)** are longer than the Ni-$S_{thioether}$ distances due to the larger radius of the selenium donor atom. The Ni-Ru distances are 3.72-3.77 Å in complex **(1)** and significantly longer at 3.92-3.98 Å in complex **(2)**.

Table 5.1: Selected bond lengths (Å) and angles (°) for the complexes **(1)** and **(2)**

Distances (Å)	**(1)**	Distances (Å)	**(2)**
Ni1-S11	2.2172(8)	Ni1-Se2	2.3295(5)
Ni1-S21	2.1913(8)	Ni1-S2	2.1970(9)
Ni1-S31	2.1677(8)	Ni1-S1	2.1728(9)
Ni1-S41	2.1669(9)	Ni1-Se1	2.2920(5)
Ni3-S12	2.229(6)	Ni2-Se3	2.3308(5)
Ni3-S22	2.196(6)	Ni2-S3	2.1890(9)
Ni3-S32	2.176(7)	Ni2-S4	2.1821(8)
Ni3-S42	2.172(7)	Ni2-Se4	2.2852(5)
Ru1-S11	2.3898(6)	Ru1-Se2	2.4997(4)
Ru1-S12	2.319(7)	Ru1-Se3	2.5124(4)
Ru1-N11	2.077(2)	Ru1-N4	2.065(3)
Ru1-N12	2.094(5)	Ru1-N2	2.075(3)
Angles (°)	**(1)**	Angles (°)	**(2)**
S11-Ni1-S41	84.84(3)	Se2-Ni1-Se1	82.506(17)
S11-Ni1-S21	85.83(3)	Se2-Ni1-S2	86.15(3)
S31-Ni1-S41	88.90(3)	S1-Ni1-Se1	88.65(3)
S21-Ni1-S31	102.98(3)	S2-Ni1-S1	103.50(3)
S11-Ni1-S41	84.84(3)	Se2-Ni1-Se1	82.506(17)
S11-Ni1-S21	85.83(3)	Se2-Ni1-S2	86.15(3)
S31-Ni1-S41	88.90(3)	S1-Ni1-Se1	88.65(3)
S21-Ni1-S31	102.98(3)	S2-Ni1-S1	103.50(3)
N11-Ru1-N21	79.59(11)	N4-Ru1-N3	79.58(11)
N12-Ru1-N22	77.2(3)	N2-Ru1-N1	79.46(10)
N12-Ru1-S11	167.9(2)	N2-Ru1-Se2	172.71(8)
N11-Ru1-S12	175.14(17)	N4-Ru1-Se3	173.27(8)
S11-Ru1-S12	90.80(15)	Se2-Ru1-Se3	88.969(13)

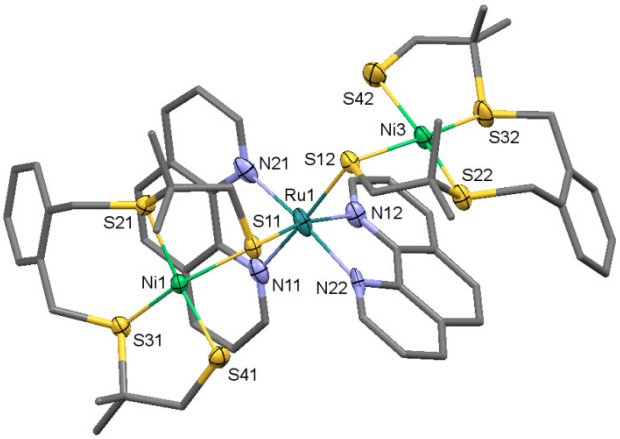

(a)

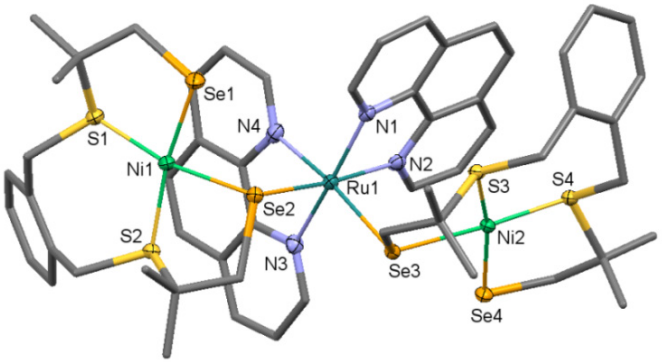

(b)

Figure 5.1: The molecular structures of (a) $[\{Ni(xbSmS)\}_2Ru(phen)_2](PF_6)_2$ and (b) $[\{Ni(xbSmSe)\}_2Ru(phen)_2](PF_6)_2$ at 110(2) K. Displacement ellipsoids (50% probability level) are shown for the atoms belonging to the first coordination spheres around the Ni and Ru metal centers. Hydrogen atoms, PF_6^- anions, lattice solvent molecules, and disorder are omitted for clarity.

5.2.3 Electrochemical Analyses

The cyclic voltammograms of the $[Ni_2Ru]$ complexes were recorded in acetonitrile solution with 0.1 M tetrabutylammonium hexafluoridophosphate as the supporting electrolyte with a scan rate of 200 mV s^{-1}. A glassy carbon electrode was used as a working electrode and Ag/AgCl was used as a reference electrode. All potentials are reported vs. the ferrocene/ferrocinium ($Fc^{0/+}$) couple ($E_{½}$ = 0.43 V vs Ag/AgCl). For both compounds **(1)** and **(2)** three irreversible reduction waves were observed with E_{pc} at −1.69, −2.05, and −2.19 V *vs*.

Fc^+/Fc for **(1)** and at −1.68, −2.04, −2.26 V *vs*. Fc^+/Fc for **(2)** (Figure 5.2a). The cyclic voltammograms of the mononuclear nickel complexes show one irreversible wave with E_{pc} at −1.96 V and −1.93 V *vs*. Fc/Fc^+ for the compounds [Ni(xbSmS)] and [Ni(xbSmSe)], respectively (Figure 5.2b). The cyclic voltammogram of *cis*-$[Ru(phen)_2(Cl)_2]$ only shows a very small reduction event, indicating that the Ru(I) oxidation state is not really accessible (Figure 5.2b). The first reduction wave for the compounds **(1)** and **(2)**, of which the peak current - compared to the second and third reduction processes - seems to indicate a two-electron process, might be assigned to the reduction of Ni^{II} to Ni^{I}. The apparent shift in the reduction potential of the nickel centers might be explained by the coordination of the dicationic ruthenium complex, the overall positive charge of the trinuclear compound making the Ni center more readily reduced.

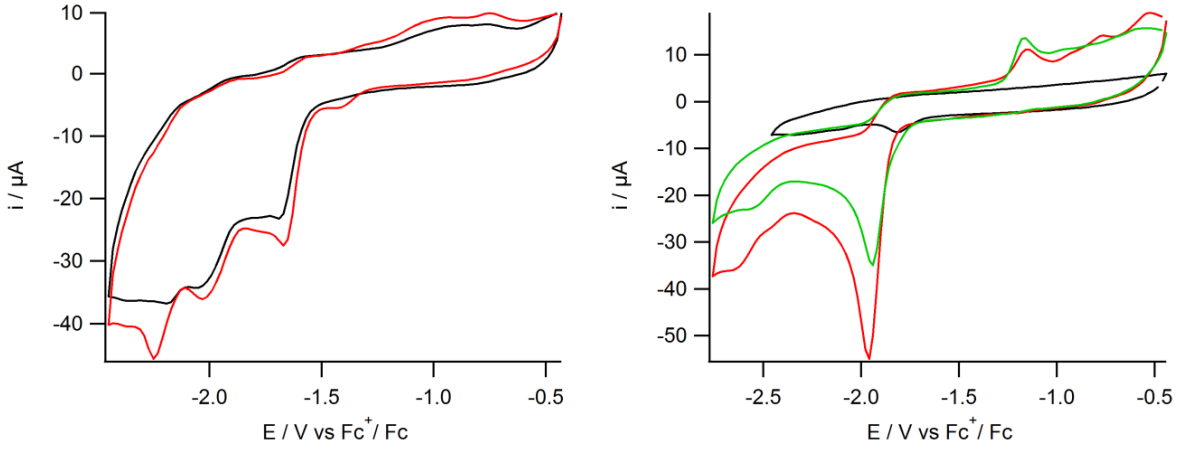

(a) (b)

Figure 5.2: Cyclic voltammograms of 1 mM solutions of (a) compound **(1)** (black) and compound **(2)** (red)**,** (b) *cis*-$[Ru(phen)_2(Cl)_2]$(black), [Ni(xbSmS)](red), [Ni(xbSmSe)](green) in acetonitrile containing $TBAPF_6$ (0.1 M) as the supporting electrolyte and a glassy carbon working electrode at 200 mV s^{-1}.

5.2.4 Electrocatalytic Hydrogen Evolution in the Presence of HOAc

The activity of the new $[Ni_2Ru]$ compounds in electrocatalytic proton reduction was studied using cyclic voltammetry by the addition of varying amounts of HOAc to acetonitrile solutions. Both complexes show electrocatalytic activity with a peak potential around −2.1 V *vs*. Fc^+/Fc, as is clear from the increasing catalytic current that appears with the addition of higher amounts of acid (Figure 5.3). The potential at which proton reduction occurs, becomes

slightly more negative at higher concentrations of acid. The overpotential for electrocatalytic proton reduction at an acetic acid concentration of 10 mM of the complexes **(1)** and **(2)** has been calculated using the half-wave potentials of the catalytic peaks, taking homoconjugation of the acid into account.[17] Both complexes display quite similar overpotentials, being 640 mV for complex **(1)** and 650 mV for complex **(2)**. In order to confirm that indeed dihydrogen gas is formed in the catalytic reaction, controlled-potential coulometry (CPC) experiments were carried out using 0.5 mM solutions of complexes **(1)** and **(2)** in acetonitrile (5 ml) in the presence of 10.5 µl of HOAc (30 equivalents of H^+ per Ni_2Ru compound) at −2.1 V *vs*. Fc^+/Fc. The quantification of produced dihydrogen gas was done volumetrically by GC analysis. The CPC experiment was run for 1 h, while the solution was stirred continuously. Using complex **(1)** as the electrocatalyst for proton reduction, a total of 49 µl (2 µmol) H_2 was produced per 0.5 mM complex in 1 h with 64% faradaic yield, whereas for complex **(2)** a total of 56 µl (2.3 µmol) H_2 was produced per 0.5 mM complex in 1 h with 63% faradaic yield. In a control experiment in the absence of the catalyst formation of H_2 is not observed at this potential.

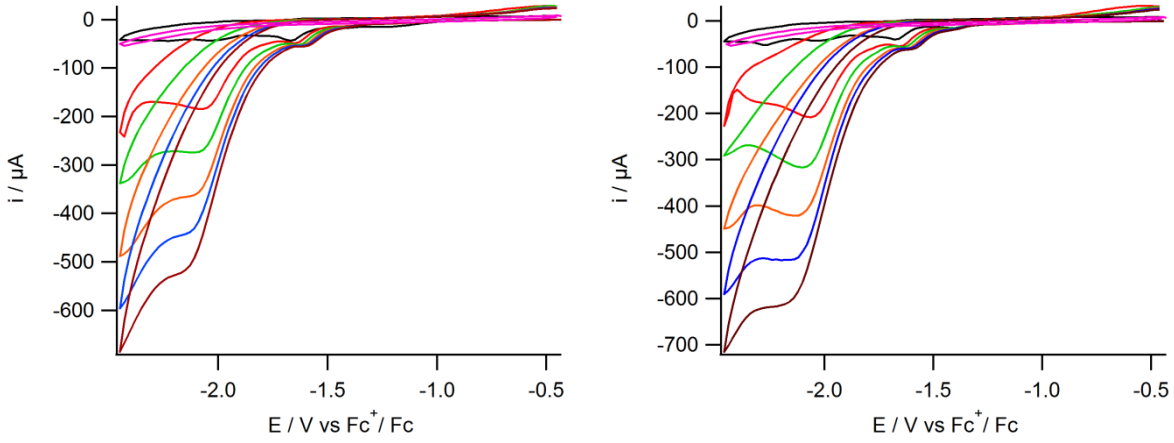

(a) (b)

Figure 5.3: Cyclic voltammograms of 1 mM solutions of (a) compound **(1)** and (b) compound **(2)** in acetonitrile containing $TBAPF_6$ (0.1 M) using a glassy carbon working electrode at 200 mV s^{-1} in the presence of 0 (black), 10 (red), 20 (green), 30 (orange), 40 (blue), 50 (brown) mM of acetic acid and blank with 50 mM of acetic acid (pink).

5.3 Discussion

In this work the compounds [{Ni(xbSmS)}$_2$Ru(phen)$_2$](PF$_6$)$_2$ **(1)** and [{Ni(xbSmSe)}$_2$Ru(phen)$_2$](PF$_6$)$_2$ **(2)** were prepared as functional mimics of the [NiFe] and [NiFeSe] hydrogenases active site. X-ray crystallography showed that the trinuclear complex cations in **(1)** and **(2)** contain two square-planar nickel centers bound in *cis* positions to the octahedral ruthenium ion via a bridging thiolate or selenolate donor atom. The electrochemical properties of the two [Ni$_2$Ru] complexes are highly similar. The substitution of the thiolate donor by a selenolate donor atom does not have a significant effect neither on the structure, nor on the electrocatalytic activity. This finding is similar to the results for the dinuclear [NiRu] compounds reported in Chapter 3. Comparison of the electrocatalytic activity of the two dicationic trinuclear complexes with that of the monocationic dinuclear [NiRu] complexes described in Chapter 3 shows that the trinuclear [Ni$_2$Ru] complexes operate at lower overpotentials, but are less efficient. The irreversibility of the reduction processes give rise to the question whether the structures are stable during catalysis. The cyclic voltammograms of the parent mononuclear nickel and ruthenium complexes are different from those of the trinuclear [Ni$_2$Ru] complexes, indicating that dissociation of the trinuclear [NiRu] compounds in solution does not occur. However, the cyclic voltammograms of both [Ni$_2$Ru] compounds show changes after the first scan (Figure AV.1-2), which might be due to partial decomposition. However, more studies should be done to gain insight concerning the electrocatalytic mechanism and active species in proton reduction.

5.4 Conclusion

Two new trinuclear compounds [{Ni(xbSmS)}$_2$Ru(phen)$_2$](PF$_6$)$_2$ and [{Ni(xbSmSe)}$_2$Ru(phen)$_2$](PF$_6$)$_2$ were synthesized with nickel complexes of tetradentate dithiolate or diselenolate ligands acting as monodentate ligands to cis-octahedral ruthenium(II) ions. Both complexes are air stable and in the presence of acetic acid catalyze the hydrogen evolution reaction as shown by CV and CPC experiments. Changing the thiolate donor atom to selenolate does not make a significant difference in the electrocatalytic activity of the resulting compounds.

5.5 Experimental

5.5.1 General

All experiments were performed using standard Schlenk techniques under a nitrogen atmosphere unless otherwise noted. Chemicals were purchased from Acros or Aldrich and were used without further purification. Organic solvents were deoxygenated by the freeze-pump-thaw method and were dried over molecular sieves prior to use. NMR spectra were recorded on a 300 MHz Bruker DPX 300 spectrometer and chemical shifts were referenced against the solvent peak. Mass spectra were obtained with a Finnigan TSQ-quantum instrument using ESI. Elemental analyses were performed by the Microanalytical Laboratory Kolbe in Germany. Electrochemical measurements were performed at room temperature under argon using an Autolab PGstat10 potentiostat controlled by GPES4 software. A three-electrode cell system was used with a glassy carbon working electrode, a platinum counter electrode and an Ag/AgCl reference electrode. All electrochemistry measurements were done in acetonitrile solution with tetrabutylammonium hexafluoridophosphate as the supporting electrolyte; after each run ferrocene was added as an internal reference. All potentials are referenced to half-wave potential of the redox couple of Fc^+/Fc, which under these conditions was found at 0.43 V *vs*. Ag/AgCl in acetonitrile, with a ΔE of 99 mV. Controlled-potential coulometry (CPC) experiments were done with the same three-electrode cell system and electrodes. CPC experiments were recorded with an Autolab PGstat10 potentiostat controlled by GPES4 software. Gas chromatographic analysis was performed on a Shimadzu gas chromatograph GC-2010 at 35 °C fitted with a Supelco Carboxen 1010 molecular sieve column. Helium was used as the carrier gas, and analytes were detected using a thermal conductivity detector operated at 80 mA. The total volume of H_2 produced during the reaction was calculated using a calibration line, which was obtained using the external reference method by injection of known amounts of H_2 into the GC using a Hamilton gas-tight syringe. A solution of complexes **(1)** or **(2)** in acetonitrile (5 ml, 0.5 mM) was placed into a three-electrode cell and prior to each measurement the system was deaerated by bubbling with helium gas for 10 min. The system was closed, and the headspace was pumped through the solution for 1 min. Before each GC sampling the headspace pumping was temporarily stopped to allow equilibration of the pressure and then GC measurement was started with a 0.5 mL sample of the headspace injection. The GC valve and the pump (KNF NMS 010 L micro diaphragm pump) were enclosed in a helium-purged housing to prevent air leaking into the system.

5.5.2 Single Crystal X-ray Crystallography

All reflection intensities were measured at 110(2) K using a SuperNova diffractometer (equipped with Atlas detector) with Cu *K*α radiation (λ = 1.54178 Å) for complex **(1)** and Mo *K*α radiation (λ = 0.71073 Å) for complex **(2)** under the program CrysAlisPro (Version 1.171.36.32 Agilent Technologies, 2013). The same program was used to refine the cell dimensions and for data reduction. The structure was solved with the program SHELXS-2014/7 and was refined on F^2 with SHELXL-2014/7.[18] Analytical numeric absorption correction using a multifaceted crystal model was applied using CrysAlisPro. The temperature of the data collection was controlled using the system Cryojet (manufactured by Oxford Instruments). The H atoms were placed at calculated positions using the instructions AFIX 23, AFIX 43 or AFIX 137 with isotropic displacement parameters having values 1.2 or 1.5 *U*eq of the attached C atoms. Both structures are partly disordered.

Additional notes on the structure determination:

(1) One of the two Ni complexes and one phenanthroline ligand coordinated to Ru are disordered over two orientations. The occupancy factors of the major components of the disorder refine to 0.543(12) and 0.550(6), respectively. The two PF_6^- counterions are found to be disordered over two orientations. The occupancy factors of the major components of the disorder refine to 0.683(4) and 0.695(4). The asymmetric unit contains 1.437 lattice acetone molecules. All solvent molecules are disordered over two orientations, but one of the two crystallographically independent solvent molecules is found at a special position.

(2) The two PF_6^- counterions are disordered over two or three orientations. All occupancy factors can be retrieved from the crystallographic information file. The crystal lattice contains some amount of lattice acetone solvent molecules. In the asymmetric unit, there is one ordered acetone molecule (with occupancy factor refining to 0.887(5)) and another acetone molecule disordered over an inversion center (and thus its occupancy factor was constrained to 0.5).

5.5.3 Synthesis of $[\{Ni(xbSmS)\}_2Ru(phen)_2](PF_6)_2$

Cis-$[Ru(phen)_2(Cl)_2]$ (0.119 g, 0.223 mmol) was dissolved in 8 ml ethanol and the solution was refluxed for 2 h. This solution was transferred, with a cannula, to a Schlenk flask containing [Ni(xbSmS)] (0.180 g, 0.446 mmol) and the resulting reaction mixture was refluxed for 24 h. After the reaction NH_4PF_6 (0.081 g, 0.496 mmol) was added to the hot ethanolic reaction mixture and the solution was stirred for 30 min, resulting in a dark reddish-

brown solid. The solid was collected by filtration in a yield of 0.155 g (0.097 mmol, 43%). ^{1}H NMR (300 MHz, $(CD_3)_2CO$) δ (ppm): 10.29 (d, Py-H), 8.71-7.17 (aromatic region), 4.12 (d, CH_2-S21/31), 4.03 (d, CH_2-S22/32), 2.33 (d, C-CH_2-S11/41), 1.64 (d, C-CH_2-S12/42), 1.47 (t, CH_3). ESI-MS (MeCN): 633.7, calcd: 633.03, $[M\text{-}2(PF_6)]^{2+}$. Elemental Analysis calcd (%) for $C_{56}H_{64}F_{12}N_4Ni_2P_2RuS_8$: C: 43.17, H: 4.14, N: 3.60; found C: 43.48, H: 4.28, N: 3.48.

5.5.4 Synthesis of $[\{Ni(xbSmSe)\}_2Ru(phen)_2](PF_6)_2$

Cis-$[Ru(phen)_2(Cl)_2]$ (0.119 g, 0.223 mmol) was dissolved in 8 ml ethanol and the solution was refluxed for 2 h. This solution was transferred, with a cannula, to a Schlenk flask containing [Ni(xbSmSe)] (0.222 g, 0.446 mmol) and the resulting reaction mixture was refluxed for 24 h. Then NH_4PF_6 (0.081 g, 0.496 mmol) was added while the reaction mixture was still hot and the solution was stirred for 30 min. After filtration a dark reddish-brown solid was obtained in a yield of 0.180 g (0.103 mmol, 46%). ^{1}H NMR (300 MHz, $(CD_3)_2CO$) δ (ppm): 10.22 (d, Py-H), 8.66-7.22 (aromatic region), 4.18 (d, CH_2-S1/2), 4.07 (d, CH_2-S3/4), 2.53 (d, C-CH_2-Se1/2), 1.65 (d, C-CH_2-Se3/4), 1.50 (t, CH_3). ESI-MS (MeCN): 727.2, calcd: 727.2 $[M\text{-}2(PF_6)]^{2+}$. Elemental Analysis calcd (%) for $C_{56}H_{64}F_{12}N_4Ni_2P_2RuS_4Se_4 \cdot 0.3C_3H_6O$: C: 38.86, H: 3.79, N: 3.16; found C: 39.12, H: 3.9,0 N: 3.08.

5.6 Acknowledgement

Mr. J.J.M. van Brussel and Mr. W. Jesse are gratefully acknowledged for performing the ESI-MS measurements.

5.7 References

1. C. Tard, C. Pickett, *J. Chem. Rev.*, 2009, **109**, 2245.
2. M. T. Koper and E. Bouwman, *Angew. Chem. Int. Ed.*, 2010, **49**, 3723.
3. M. Stephenson, L. H. Stickland, *Biochem J.*, 1931, **25(1)**, 205.
4. T. R. Simmons, G. Berggren, M. Bacchi, M. Fontecave and V. Artero, *Coord. Chem. Rev.*, 2014, **271**, 127.
5. G. M. Chambers, M. T. Huynh, Y. Li, S. Hammes-Schiffer, T. B. Rauchfuss, E. Reijerse and W. Lubitz, *Inorg. Chem.*, 2016, **55**, 419.
6. S. Canaguier, M. Fontecave and V. Artero, *Eur. J. Inorg. Chem.*, 2011, 1094.
7. S. Canaguier, L. Vaccaro, V. Artero, R. Ostermann, J. Pecaut, M. J. Field and M. Fontecave, *Chem. Eur. J.*, 2009, **15**, 9350.
8. Y. Oudart, V. Artero, L. Norel, C. Train, J. Pécaut and M. Fontecave, *J. Organomet. Chem.,* 2009, **694**, 2866.
9. Y. Oudart, V. Artero, J. Pécaut, C. Lebrun and M. Fontecave, *Eur. J. Inorg. Chem.*,

2007, 2613.
10. G. M. Chambers, R. Angamuthu, D. L. Gray and T. B. Rauchfuss, *Organometallics*, 2013, **32**, 6324
11. E. Garcin, X. Vernede, E. Hatchikian, A. Volbeda, M. Frey and J. Fontecilla-Camps, *Structure* 1999, **7**, 557.
12. C. Wombwell and E. Reisner, *Chem. Eur. J.* 2015, **21**, 8096.
13. G. Gezer, D. Durán Jiménez, M. A. Siegler and E. Bouwman, *Dalton Trans.*, 2017, **46**,7506.
14. J. A. Verhagen, D. D. Ellis, M. Lutz, A. L. Spek and E. Bouwman, *Dalton Trans.,* 2002, 1275.
15. C. Wombwell and E. Reisner, *Chem. Eur. J.* 2015, **21**, 8096.
16. J. E. Collins, J. J. S. Lamba, J. Christopher Love, J. E. McAlvin, N. Christina, B. P. Peters, W. Xufeng and C. L. Fraser, *Inorg. Chem*, 1999, **38**, 2020.
17. V. Fourmond, P. A. Jacques, M. Fontecave and V. Artero, *Inorg. Chem.*, 2010, **49**, 10338.
18. G. M. Sheldrick, *Acta Cryst*, 2015, **C71**, 3.